Solution Structure of the Minor Conformer of a DNA Duplex Containing a dG Mismatch Opposite a Benzo[*a*]pyrene Diol Epoxide/dA Adduct: Glycosidic Rotation from Syn to Anti at the Modified Deoxyadenosine†

J. L. Schwartz,‡ J. S. Rice,‡ B. A. Luxon,‡ J. M. Sayer,§ G. Xie,§ H. J. C. Yeh,§ X. Liu,§ D. M. Jerina,§ and D. G. Gorenstein*,‡

Sealy Center for Structural Biology and Department of Human Biological Chemistry and Genetics, University of Texas Medical Branch, Galveston, Texas 77555-1157, and National Institute of Diabetes and Digestive and Kidney Diseases, National Institutes of Health, Bethesda, Maryland 20892-0820

Received June 2, 1997; Revised Manuscript Received July 25, 1997⊗

ABSTRACT: Polycyclic aromatic hydrocarbons (PAHs) are widespread environmental contaminants whose metabolism in mammals results in deleterious cell transformation. Covalent modification of DNA by diol epoxides metabolically formed from PAHs such as benzo[*a*]pyrene (BaP) provides a mechanism for the genotoxicity, mutagenicity, and carcinogenicity of PAHs. We had previously reported NMR evidence for a minor conformer of the duplex d($G_1G_2T_3C_4A_5$*$C_6G_7A_8G_9$)·d($C_{10}T_{11}C_{12}G_{13}G_{14}G_{15}A_{16}C_{17}C_{18}$) containing a dG_{14} mismatch opposite a dA_5* residue modified at the exocyclic amino group by trans addition to (+)-(7*R*,8*S*,9*S*,10*R*)-7,8-dihydroxy-9,10-epoxy-7,8,9,10-tetrahydrobenzo[*a*]pyrene [Yeh, H. J. C., Sayer, J. M., Liu, X., Altieri, A. S., Byrd, R. A., Lashman, M. K., Yagi, H., Schurter, E. J., Gorenstein, D. G., & Jerina, D. M. (1995) *Biochemistry 34,* 13570−13581]. In the present work, we describe the structure of this minor conformer (ca. 17% of the total conformer population). This represents the first structural determination of a minor conformer of a carcinogen-lesion DNA adduct. Two-dimensional NOESY, ROESY, TOCSY, and exchange-only spectra at 750 MHz allowed nearly complete sequential assignment of both conformers. In the minor conformer, the adducted base assumes an anti-glycosidic torsion angle whereas in the major conformer it assumes an unusual syn-glycosidic torsion angle. The aromatic hydrocarbon in the minor conformer is intercalated between dG_{13} and dG_{14}, preserving the energetically favorable stacking interactions found in the major conformer. The major structural differences between the two conformers appear to be near the lesion site as evidenced by the large chemical shift differences between major and minor conformer protons near the lesion site; away from this site, the chemical shifts of the major and minor conformer protons are nearly identical. Because any of the conformations of benzo[*a*]pyrene diol epoxide-modified DNA may contribute to tumorigenic activity, structural determination of all conformations is essential for the elucidation of the mechanism of cell transformation initiated by covalent modification of DNA by PAHs.

Although substantial data exist on the reactivity of the carcinogenic polycyclic aromatic hydrocarbon diol epoxides (DE) with DNA and on the structures of the modified duplexes formed (Geacintov et al., 1997; Jerina et al., 1996), there has been no obvious correlation of tumorigenicity with either overall chemical reactivity, efficiency of covalent binding to DNA as opposed to hydrolysis, or relative proportions of dG *vs* dA adducts or of cis *vs* trans epoxide ring opening for specific diol epoxides (Jerina et al., 1991). For a number of diol epoxides derived from different hydrocarbons, the (*R*,*S*,*S*,*R*)-DE2 isomer (*R* configuration at the benzylic epoxide carbon and trans orientation of the epoxide oxygen relative to the benzylic hydroxyl; cf. Figure 1) is both the predominant diol epoxide formed metabolically and the most tumorigenic (Jerina et al., 1984). In contrast, the DE1 isomers (cis orientation of the epoxide oxygen and benzylic hydroxyl) and the (*S*,*R*,*R*,*S*)-DE2 isomer are generally not tumorigenic or only weakly so. What are the structural and dynamic features that make the (*R*,*S*,*S*,*R*)-DE2 isomer so carcinogenic?

We previously reported (Yeh et al., 1995) the solution structure of the major conformer of the deoxyoligonucleotide duplex

d($G_1G_2T_3C_4A_5$*$C_6G_7A_8G_9$)·
d($C_{10}T_{11}C_{12}G_{13}G_{14}G_{15}A_{16}C_{17}C_{18}$)

with a synthetic deoxyadenosine adduct [trans DE2(10*S*) dA adduct = dA_5*] corresponding to trans ring opening by the exocyclic amino group at the benzylic C10 of the most tumorigenic benzo[*a*]pyrene (BaP) DE isomer, (+)-(7*R*,8*S*,9*S*,10*R*)-7,8-dihydroxy-9,10-epoxy-7,8,9,10-tetrahydrobenzo[*a*]-pyrene [(+)-(*R*,*S*,*S*,*R*)-DE2] (Figure 1). This duplex was constructed with a dG_{14} base in the complementary strand opposite the trans DE2(10*S*) dA adduct, since we had observed that this mismatched duplex was more stable than

† This research was supported in part by the NIH (AI27744), the NIEHS (ES06676, R01 ES06839), the Welch Foundation (H-1296), the Lucille P. Markey Foundation, and the Sealy and Smith Foundation. Building funds were provided by the NIH (1CO6CA59098).

* Author to whom correspondence should be addressed: University of Texas Medical Branch, Sealy Center for Structural Biology, Dockside Building, Galveston, TX 77555-1157. Telephone: 409-747-6801. Facsimile: 409-747-6850. E-mail: david@nmr.utmb.edu.

‡ University of Texas Medical Branch.

§ National Institutes of Health.

⊗ Abstract published in *Advance ACS Abstracts,* August 15, 1997.

S0006-2960(97)01306-8 CCC: $14.00

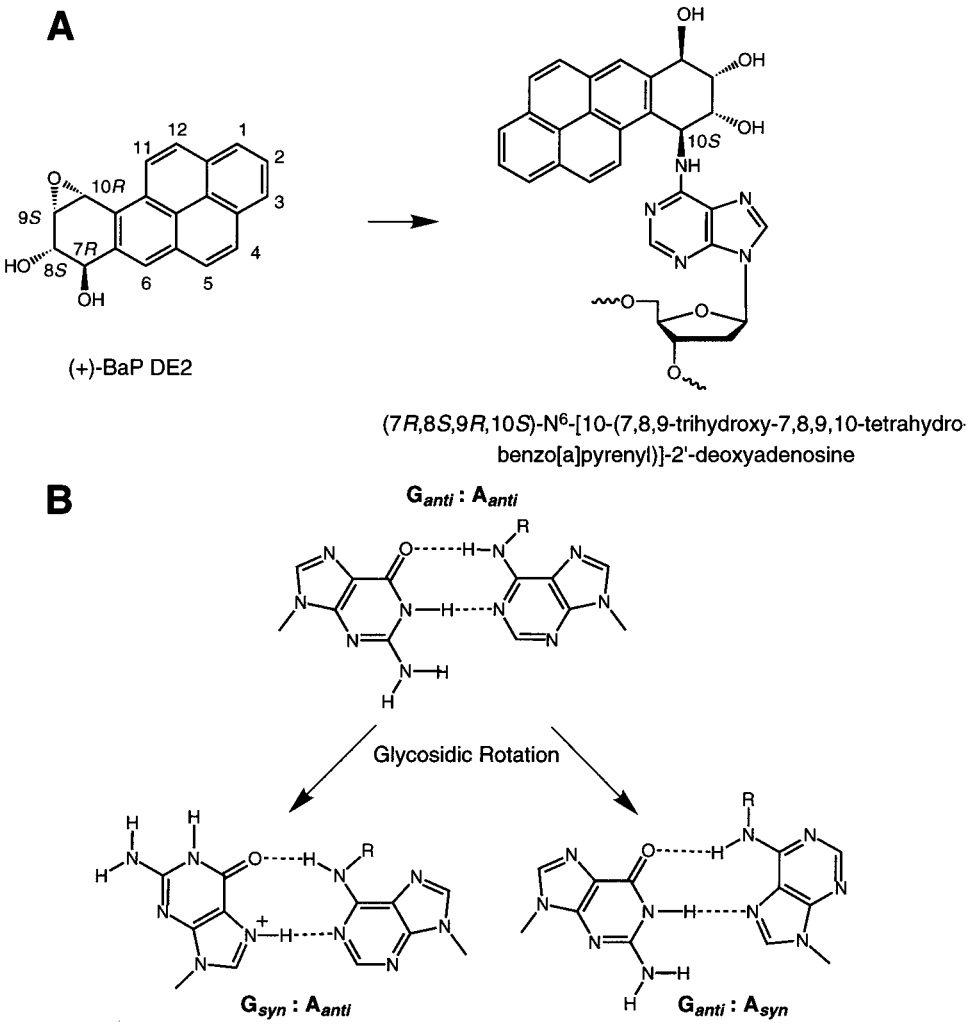

FIGURE 1: (A) Structure of the adduct derived from trans addition of the exocyclic N^6-amino group of deoxyadenosine to (+)-(7*R*,8*S*,9*S*,10*R*)-7,8-dihydroxy-9,10-epoxy-7,8,9,10-tetrahydrobenzo[*a*]pyrene [(+)-DE2]. (B) Possible base pair orientations for the dA-dG pair. The orientation of the dA_5*-dG_{14} base pair for the minor conformer is dA_{anti}-dG_{anti}, whereas for the major conformer it is dA_{syn}-dG_{anti}.

the duplex with a dT opposite dA_5* ($\Delta T_m = 11$ °C) (Schurter et al., 1995). At that time we noted the presence of a minor conformer that represented 17% of the total conformer population (Yeh et al., 1995). Because minor or less populated conformations of diol epoxide−DNA adducts may promote tumorigenic activity, we feel it is essential that the structures of both the major and minor conformers be determined. In this paper we report the first structure determination of a minor conformer.

MATERIALS AND METHODS

Sample Preparation. A previously published synthetic approach for the incorporation of diol epoxide modified dA phosphoramidites into oligonucleotides was used (Yeh et al., 1995) to synthesize the nonamer d(GGTCA*CGAG). The modified strand was titrated with the complementary strand d(CTCGGGACC), and the end point (1:1 ratio) was determined spectroscopically as described (Yeh et al., 1995). For the NMR studies, approximately 180 A_{260} units of the duplex was dissolved in 500 μL of a buffer consisting of 12 mM Na_2HPO_4, 8 mM NaH_2PO_4, and 56 mM NaCl with a trace of sodium azide. The final pH was 6.8.

NMR Experiments. Varian UnityPlus 600 and 750 MHz spectrometers at a regulated temperature of 15 °C were used to record 2D NOESY, ROESY, TOCSY, and exchange-only spectra. The sample was prepared in either 99.999% D_2O or 90% H_2O/10% D_2O buffer. *Z*-filtered TOCSY (Rance, 1987) spectra were recorded with 30 and 80 ms mixing times, and ROESY (Bothner-By et al., 1984; Bax & Davis, 1985) and exchange-only (Macura et al., 1994; Gejzo et al., 1991) spectra were recorded with 200 ms mixing times. The 99.999% D_2O and 90% H_2O/10% D_2O 750 MHz NOESY spectra were recorded with 200 ms mixing times in the hypercomplex, phase-sensitive mode with 4096 complex points in t_2 and 376 and 512 complex points in t_1, respectively, with sweep widths of 6554 and 15004 Hz, respectively. The data were processed with a 90° shifted sine-bell weighting function. The relaxation delay was 4.0 s for the 99.999% D_2O NOESY and 2.8 s for the 90% H_2O/10% D_2O NOESY.

NOESY Distance-Restrained Molecular Dynamics Calculations on the Adduct. The NMR structural refinement used a MORASS/AMBER protocol similar to that previously described (Schurter et al., 1995). Calculations were performed on a Silicon Graphics Indigo2 workstation. The hybrid relaxation matrix program, MORASS 2.2 (Meadows et al., 1996) was used to generate 188 nonexchangeable proton NOE constraints. Seventy exchangeable proton NOE constraints were generated by assigning weak (4.7−5.7 Å), medium (2.7−4.7 Å), and strong (1.7−2.7 Å) intensities to

cross peaks in the 90% H_2O/10% D_2O 750 MHz NOESY spectrum. A total of 274 NOESY flat-well distance constraints [188 nonexchangeable, 70 exchangeable, and 16 5.0 kcal/(mol·Å^2) imino H-bonds (*vide infra*)] were used for iterative refinement using distance-restrained molecular dynamics (rMD) calculations with a locally modified version of AMBER 4.1 MINMD (Pearlman et al., 1995). This modification consisted solely of the introduction of two harmonic half-well potentials in order to produce a "flat well" between these two potentials with zero energy penalty and the requisite code to manage the flat-well atoms list. The final structure of the major conformer of the adduct (Yeh et al., 1995) was used as the starting model for the MORASS/restrained MD calculations. The MIDAS Plus molecular interactive display program (Ferrin et al., 1988) was used to manipulate and display the structures.

Convergence of this short 9-mer duplex structure was difficult to achieve, presumably due to electrostatic end effects. In order to minimize these effects, a tetramer duplex (ACGT) was added to both ends of the 9-mer, thereby making it a 17-mer during the refinement process (with 16 imino H-bonds: the dA_5*-dG_{14} imino was not restrained). After achieving convergence with this 17-mer, the tetramers were removed and the resulting 9-mer was energy minimized to give the final structure.

All energy minimization and restrained molecular dynamics calculations were done *in vacuo* with an 8 Å cutoff distance-dependent dielectric to simulate water solvation. At each iteration the recalculated flat-well restraints generated by MORASS were annealed into the 17-mer model structure via rMD by raising the temperature from 300 to 900 K for 2 ps while using the "belly" option on the four base pairs at each end to fix their positions. Subsequently, the temperature was reduced first to 500 K over 2 ps and then to 300 K over 2 ps while using the belly option. The final run consisted of 50 ps of rMD with the belly option turned off. The coordinates for the last 40 ps of this MD run were averaged using CARNAL (Ross, 1994), followed by 2000 steps of full conjugate gradient minimization with the NOESY restraints on. This completed one cycle of refinement. This process was repeated until a satisfactory agreement between the calculated and observed cross-peak volumes were obtained: in this study, nine iterations were performed.

Convergence was monitored by using eqs 1 and 2; RMS = root mean square.

$$\%\ \mathrm{RMS}_{\mathrm{vol}} = \{(1/N)\sum[(v_{ij}^{a} - v_{ij}^{b})/v_{ij}^{a}]^2\}^{1/2} \times 100 \quad (1)$$

% $\mathrm{RMS}_{\mathrm{vol}}$ = % T when v_{ij}^{a} = the calculated volume and v_{ij}^{b} = the experimental volume and % $\mathrm{RMS}_{\mathrm{vol}}$ = % E when v_{ij}^{a} = the experimental volume and v_{ij}^{b} = the calculated volume. N = the number of NOE volumes.

$$R^{1/6} = \{(1/N)\sum[(v_{ij}^{a1/6} - v_{ij}^{b1/6})/v_{ij}^{a1/6}]^2\}^{1/2} \quad (2)$$

$R^{1/6}$ = percent root mean square difference in the $^1/_6$th power of the volumes when v_{ij}^{a} = the calculated volume and v_{ij}^{b} = the experimental volume. Convergence was achieved when the % $\mathrm{RMS}_{\mathrm{vol}}$ and $R^{1/6}$ were within the reliability of the experimental volume measurement.

RESULTS

Sequential connectivity assignments at 750 MHz were performed with the aid of 2D NOESY and TOCSY experiments (Figure S1) using established methods for canonical B-DNA (Wüthrich, 1986). Assignments for the major conformer were previously reported (Yeh et al., 1995). Chemical shifts for the minor conformer and chemical shift differences between the conformers are reported in Tables S1, 1, and 2. The most dramatic chemical shift changes between equivalent resonances in the major and minor conformers are found near the intercalation site, particularly those resonances found in dC_4, dA_5*, dC_6, and dG_{14} (imino proton) (Table 2). Especially noteworthy are the chemical shifts for the two dA_5* base protons (H_2 of the major and H8 of the minor conformer) which appear as an incompletely resolved pair of signals at ~8.7 ppm. Corresponding signals are observed at 7.93 ppm for H2 of the minor conformer and 7.81 ppm for H8 of the major conformer. These constitute the largest chemical shift differences observed between the major and minor conformers. Residues not close to the intercalation site show little difference in chemical shift between the two conformers, indicating that the major structural changes between the major and minor conformer occur very close to the intercalation site. Because of the small differences in the chemical shifts between many of the protons in the two conformers, assignment at 750 MHz proved essential. NOE volumes were used in concert with a full hybrid relaxation matrix analysis using MORASS 2.2 (Meadows et al., 1996) to obtain distance restraints (Table S2) for restrained molecular dynamics calculations using a locally modified version of AMBER 4.1 MINMD (Pearlman et al., 1995). Refinement proceeded normally with a final % $\mathrm{RMS}_{\mathrm{vol}}$ = 80% and $R^{1/6}$ = 7.4% by the ninth iteration (Table S3). In both conformers, the aromatic ring of the benzo[a]pyrene intercalates from the major groove on the 3′ side of the modified adenine. In contrast to the major conformer, the adenine ring of dA_5* in the minor conformer adopts the more common anti-glycosidic conformation and forms an anti−anti base pair with dG_{14} maintained by two hydrogen bonds (Figures 1 and 2). Extensive NMR evidence supports the anti−anti base pair conformation in the minor conformer:

(1) The intensity of the H8−H1′ NOE is consistent with an anti orientation for dA_5* whereas the unusually intense H8−H1′ NOE for the major conformer supports the presence

Table 1: Chemical Shift Assignments of the Hydrocarbon Moiety and Chemical Shift Difference between the Major and Minor Conformers: $\Delta = \delta_{\mathrm{minor}} - \delta_{\mathrm{major}}$ (ppm)[a]

proton	δ_{major}	δ_{minor}	Δ
H1	7.49	7.59	0.10
H2	7.60	7.66	0.06
H3	7.82	7.85	0.03
H4	7.31	7.17	−0.14
H5	6.93	6.95	0.02
H6	7.76	7.83	0.07
H7	5.13	5.11	−0.02
H8	3.89	3.85	−0.04
H9	4.28	4.55	0.27
H10	5.66	6.14	0.48
H11	6.38	6.47	0.09
H12	6.64	6.91	0.27

[a] The assignments for the major conformer were obtained from a previous study (Yeh et al., 1995). However, the actual chemical shifts reported here were obtained from the data in this study. To accurately compare both conformer chemical shifts, the minor conformer chemical shifts were referenced to the major conformer dC_{17} H5−H6 NOE cross peak (reported as 5.18 and 7.18 ppm, respectively).

Table 2: Chemical Shift Difference between Major and Minor Conformers: $\Delta = \delta_{minor} - \delta_{major}$ (ppm)[a]

residue	H1′	H2′	H2″	H3′	H4′	H6/H8	H5	H2	CH_3	NH	NH_2[b]
dG_1											
dG_2	0.02	0.01	0.01	0.02		0.02					
dT_3	0.05	−0.03	0.03			−0.01			0.02	0.05	
dC_4	0.35	−0.75	0.45	−0.01		−0.12	0.19				0.04/0.19
dA_5*	0.16	0.62	0.34	−0.52	0.29	0.92		−0.79			0.18
dC_6	0.18	−0.12	−0.02	0.15		−0.14	0.01				0.04/−0.11
dG_7	−0.08	0.01	−0.02			0.02				−0.02	
dA_8	0.00	−0.01	0.00			−0.01		−0.02			
dG_9	0.00	0.00	0.00			0.00					
dC_{10}	0.00	0.00	0.00			0.00	0.00				
dT_{11}	0.00	0.00	0.00			0.00			−0.01	−0.06	
dC_{12}	−0.03	0.14	0.06	0.01		0.03	−0.03				−0.07/−0.04
dG_{13}	−0.03	−0.02	0.00			−0.04				0.05	
dG_{14}	0.05					−0.02				−0.45	−0.07[c]
dG_{15}	−0.02	0.00	0.00			0.01				−0.09	
dA_{16}	0.02	0.02	0.01			0.03					
dC_{17}	0.03					0.01	0.01				
dC_{18}	0.00					0.00	0.00				

[a] The assignments for the major conformer were obtained from a previous study (Yeh et al., 1995). However, the actual chemical shift differences reported here were obtained from the data in this study. Only the differences for those protons that were not completely overlapped with the major conformer are reported. [b] Bonded/nonbonded. [c] These amino protons are degenerate.

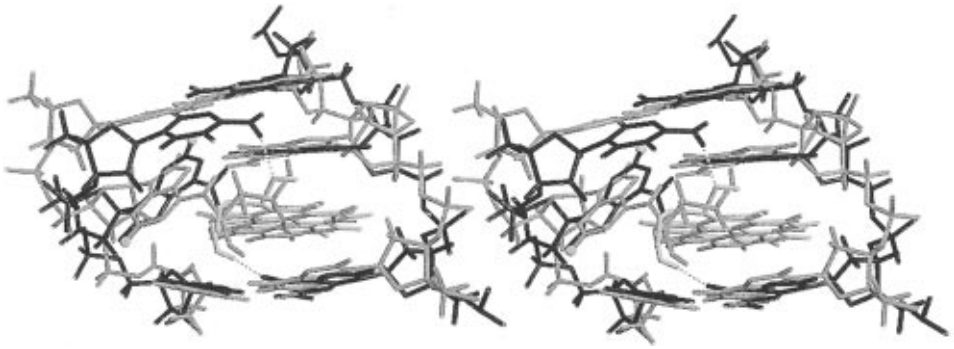

FIGURE 2: Stereoview overlay of the central three base pairs (dC_4-dG_{15}, dA_5*-dG_{14}, and dC_6-dG_{13}) of both the minor and major conformers. The minor conformer is blue with an orange adduct while the major conformer is in green. To illustrate the difference in the anti (minor conformer) and syn (major conformer) glycosidic conformation, the H2 protons are shown as red spheres. The dashed yellow lines illustrate two hydrogen bonds in the minor conformer between the dC_4 nonbonded amino proton and the hydroxyl oxygen at position 7 of the hydrocarbon and between the hydroxyl proton at position 9 of the hydrocarbon and dG_{13} O6.

of a syn conformation for the major conformer (Figure S1) (Yeh et al., 1995; Wüthrich, 1986). NOEs for mismatch paired dG_{14} support an anti conformation for this residue in both conformers of the duplex; i.e., dG_{14} has not rotated in one conformer relative to the other.

(2) We observe relatively intense NOEs (corrected for the major/minor ratio) between the dA_5* H8 and both the dA_5* H2′ and H2″, indicating the normal anti configuration for dA_5*.

(3) NOEs between the dA_5* H2 proton and the dG_{14} imino and amino protons were observed in a 90% H_2O/10% D_2O solution, indicating that these protons are close in space (within ~5 Å) as they would be in an anti−anti base pair (Figure 1). However, the corresponding NOEs are not detected in the major conformer, which has an unusual syn−anti base pair as evidenced by the NOE between the dA_5* H8 proton and the dG_{14} imino proton (data not shown).

(4) The chemical shifts for H8 (8.73 ppm) and H2 (7.93 ppm) of dA_5* in the minor conformer are consistent with an anti conformation as observed in other DNA duplexes. Reversal of the relative positions of the chemical shifts for these two protons is observed in the major conformer, which has a syn orientation of dA_5*.

The aromatic hydrocarbon in the minor conformer is intercalated between dG_{13} and dG_{14}, preserving the energetically favorable stacking interactions found in the major conformer. This intercalation is supported by NOEs between the protons of the pyrene ring system and several base and sugar protons on dG_{13} and dG_{14}.

DISCUSSION

Comparison of the Major and Minor Conformers. The principal difference between the two conformations is the syn/anti orientation of dA_5*. This appears to have a significant effect on the structure of the duplex surrounding the lesion with the relative positions of the residues of the modified strand being significantly altered between the major and minor conformers (Figure 2). In the major conformer, the adenine of dA_5* appears to project more into the major groove than it does in the minor conformer. In our restrained MD simulations we could readily convert the initial syn dA_5* conformer to the anti conformer by placing the observed NOE distance restraints on the dA_5* base to the adjacent nucleotides and heating to 300 K. Within the first 2 ps, the dA_5*-dG_{14} hydrogen bonds are broken and the separation between the dA_5*-dG_{14} and the dC_6-dG_{13} base pairs widens to accommodate a rotating dA_5* as it converts from a syn to an anti conformation. Upon rotation from syn to anti, the dA_5* base reorients itself from making a hydrogen bond between its N7 and the dG_{14} imino proton to a position in

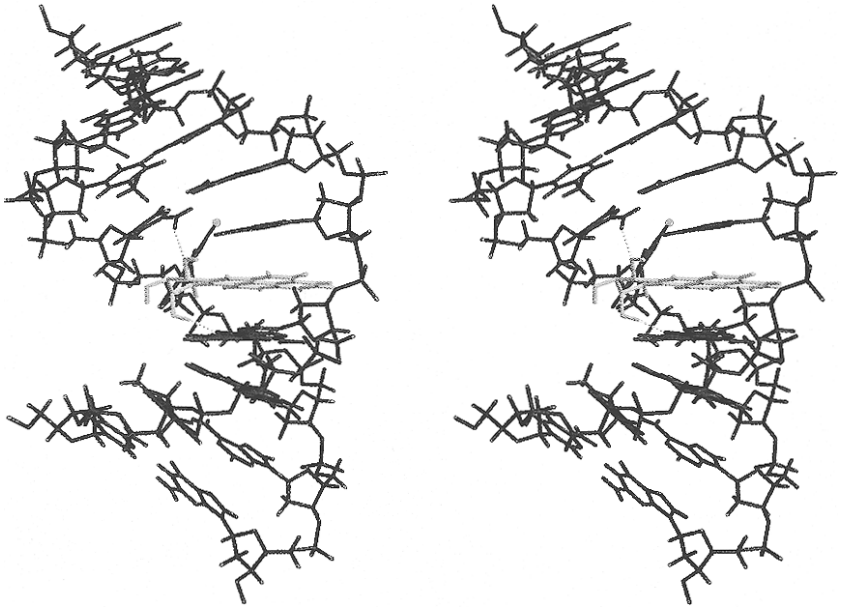

FIGURE 3: Stereoview of the minor conformer duplex. The dashed yellow lines illustrate two hydrogen bonds in the minor conformer between the dC_4 nonbonded amino proton and the hydroxyl oxygen at position 7 of the hydrocarbon and between the hydroxyl proton at position 9 of the hydrocarbon and dG_{13} O6.

which it can make a hydrogen bond between its N1 and the dG_{14} imino proton. In the process, the dG_{14} base maintains a coplanar relationship with the pyrene ring system, which moves very little during this process. In addition, the relative position of dG_{14} to dG_{15} has not changed significantly, and the positions of the backbone atoms are similar between the major and minor conformers in the unmodified strand (Figure 2). This simulation suggests that syn−anti interconversion does not require the hydrocarbon to become extrahelical and allows it to retain its intercalation geometry throughout the entire process. The similarity in the structures of the unmodified strands of the major and minor conformers is reflected in the minimal chemical shift differences at dG_{13}, dG_{14}, and dG_{15} (Table 2). The large difference in chemical shift for the imino proton of dG_{14} for the two conformers is likely due to the difference in hydrogen-bonding partners on dA_5*: N7 versus N1.

In support of the facile interconversion of dA_5* between syn and anti conformers, exchange cross peaks between the major and minor conformers at both the H8 and H2 positions of dA_5* and H10 and H12 of the hydrocarbon were established by 2D ROESY (Bothner-By et al., 1984; Bax & Davis, 1985) and exchange-only (Macura et al., 1994; Gejzo et al., 1991) experiments (spectra not shown). This conformational exchange is slow enough on the NMR time scale (rate less than the chemical shift difference between the two conformers, $<94\ s^{-1}$) that separate cross peaks due to different chemical environments for these protons are observed.

The direction of the chemical shift changes between the conformers for the H2 and H8 protons on dA_5* can be correlated with the structural change due to the dA_5* base rotation (*vide supra*). However, while the dC_4 or other dA_5* protons exhibit some of the largest chemical shift changes between the major and minor conformers, the directions of these changes do not appear to be due exclusively to the difference in positions between these protons and the dA_5* base or the hydrocarbon. With a dynamic dA_5* base and the limited resolution of this structure, we have found that there is not a simple correlation between the directions of these chemical shift changes and structural differences between the conformers. In addition, the hydrocarbon is too far away from these protons in either of the structures to cause these chemical shift changes.

In the major conformation the duplex has B-DNA character with the base pairs perpendicular to the helix axis except near the intercalation site, where the duplex bends about 20−30°. However, in the minor conformation, the duplex has the appearance of an A-like DNA structure in the region surrounding the lesion, with a larger bend in the helix axis (∼45°) at the dA_5*-dG_{14} mismatch (Figure 3). The Cartesian RMSD (root mean square deviation) between the two structures is 2.14 Å, largely reflecting the difference in the degree of bend in the helix axis. Of course, it is important to emphasize that it is very difficult to define the long-range bend of a duplex on the basis of the short-range NOEs we can determine between nearest nucleotide neighbors. In addition, this is only a moderate resolution structure with a % RMS_{vol} of 80% and an $R^{1/6}$ of 7.4% (Table S3). The larger error reflects the difficulty in integrating minor conformer cross peaks which are $^1/_6$th the intensity of the major conformer cross peaks and the proximity of the much larger major conformer cross peaks to the minor conformer cross peaks. In addition, there may be some degree of magnetization transfer associated with conformational exchange between the two conformers.

In the major conformer, base stacking is observed between dC_4 and dA_5*. In contrast, there is a significant loss of stacking between these bases in the minor conformer (Figure 4), as well as a large displacement of the dC_4/dA_5* phosphorus positions. Loss of base stacking is due to a translation of the dC_4 base from a position in which it is above the dA_5* base to one in which it is closer to the aliphatic portion of the hydrocarbon. Thus, in the minor conformer, we observe NOEs between the dC_4 H5 and H6 protons and both the H8 and H9 protons of the hydrocarbon. The corresponding NOEs appear to be absent for the major conformer where the dC_4 base is over the dA_5* base and

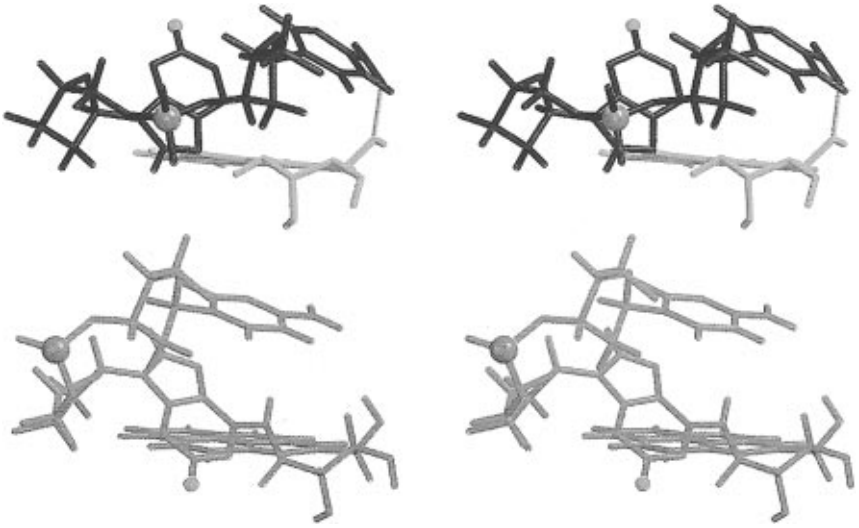

FIGURE 4: Stereoview of dC_4 and dA_5* of both the minor (top) and major (bottom) conformers illustrating the loss of base stacking in the minor conformer compared to the major conformer and the large displacement in the backbone position between both conformers. The purple spheres represent the dC_4pdA_5* phosphorus atoms. The minor conformer is in blue with an orange adduct while the major conformer is in green. To illustrate the difference in the anti (minor conformer) and syn (major conformer) glycosidic conformations, the H2 protons are shown as red spheres. The yellow line illustrates the hydrogen bond in the minor conformer between the dC_4 nonbonded amino proton and the hydroxyl oxygen at position 7 of the hydrocarbon.

thus well away from the aliphatic portion of the hydrocarbon. This difference in dC_4/dA_5* base stacking may contribute to the difference in relative conformer populations.

As shown in Figures 2 and 3, in the minor conformer, partial unwinding and bending of the helix at the lesion site are required to retain the hydrocarbon intercalation geometry and to retain two H-bonds for the dA_5*-dG_{14} mismatch. In addition, this distortion allows formation of a new H-bond between the hydroxyl oxygen at C7 of the BaP moiety and the nonbonded amino proton of dC_4 (*vide infra*). The distortion of the minor conformer duplex is likely associated with the putative bend introduced at the junction of the dA_5*/dC_4 bases (Figure 4).

Interatomic distances consistent with hydrogen bonding between the DNA bases and hydroxyl groups of the BaP moiety in both the major and the minor conformer are observed. In both conformers, there is a hydrogen bond between the DE hydroxyl proton at C9 and O6 of dG_{13} in the complementary strand. In the major conformer, there is a H-bond between the DE hydroxyl proton at C7 and dG_{14} N7, whereas this is absent in the minor conformer. However, in the minor conformer, a new H-bond is formed between the DE hydroxyl oxygen at C7 and the dC_4 nonbonded amino proton. These H-bonds between the BaP moiety and the DNA bases above and below it may explain the relative stability of the minor conformer and the kinetic barrier for transition between the conformers.

These H-bonds between the ring hydroxyl groups and the neighboring bases place strict stereochemical requirements at carbons 7 and 9. In the trans DE2(10*S*) dA adduct, the hydroxyls at C7 and C9 are properly oriented to allow a H-bond bridge between the base pairs above and below the adducted dA. Epimerization of either center would eliminate one or both of these H-bonds (assuming no major reorganization of the hydrocarbon and duplex geometry). Thus the requirement for structure-stabilizing features such as these H-bonds could explain the unique behavior of this adduct. Of the structures studied to date (Geacintov et al., 1997; Jerina et al., 1996) the trans DE2(10*S*) dA adduct described here is the first to be documented to have well-resolved, separable signals for both a major and minor conformer. Without the additional stabilization of the minor conformer and increased energy barrier for transition between conformers created by the H-bonds to the neighboring bases, exchange between the various conformers may be more facile, leading to averaged, broadened lines, as observed for some other adduct stereoisomers. A possible requirement for specific H-bonding partners at base pairs above and below the adducted base could also explain some of the sequence dependence of the biological behavior of these lesions, such as hot spots for mutagenicity and carcinogenicity.

Origin of Conformational Heterogeneity in 10S Adducts. In the one case to date where it has been possible to obtain and compare NMR structures of oligonucleotides containing *R* and *S* dA adducts of a PAH diol epoxide (benzo[*c*]-phenanthrene) (Cosman et al., 1993, 1995) with a complementary dT, one or more minor conformers were apparent for the oligonucleotide duplex containing the *S* adduct, whereas the *R* adduct showed a single conformation. Results to date (Schurter et al., 1995; Zegar et al., 1996; Liu et al., in preparation) with BaP DE adducts are also consistent with the generalization that 10*R* dA adducts opposite dT are conformationally homogeneous. In contrast, the 10*S* adducts from BaP diol epoxides with a complementary dT opposite the adducted dA have proven intractable to NMR study because of line broadening and/or multiple signals due to different chemical environments of a single proton. Furthermore, oligonucleotide duplexes containing 10*S* dA adducts of BaP diol epoxides opposite dT consistently exhibit lower T_m values than the corresponding duplexes containing 10*R* adducts. All these differences are consistent with a greater degree of conformational flexibility for the 10*S* adducts and are presumably related to the different orientation of the hydrocarbon in the two isomers. Figure 5 illustrates the relative orientation of the hydrocarbon and the modified adenine in trans 10*R* (Zegar et al., 1996; Liu et al., in preparation) and 10*S* (this work) DE2 dA* adducted duplexes with anti conformation of the adducted dA* residues and

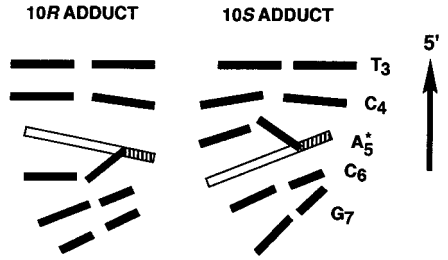

FIGURE 5: Schematic representation of the orientation of the hydrocarbon and the adducted adenine base relative to adjacent base pairs in the minor conformation of the trans DE2(10*S*) dA adduct (this work) and a typical trans DE2(10*R*) dA adduct. Note that both adduct duplexes have the modified dA* in the anti conformation. The 5′ end of the adducted strand is at the top. These drawings are rotated ~180° about the helix axis relative to the molecular models in Figures 2−4. The cross-hatched portion of the hydrocarbon represents the tetrahydro ring.

base pairing between the adducted dA* and its opposing base (dT in the 10*R* and dG in the 10*S* adduct). The aromatic ring system is intercalated toward the 3′ end of the modified strand in the 10*S* adducted duplexes and toward the 5′ end in the 10*R* adducted duplexes. Notably, in the two configurations, the hydrocarbon and the modified adenine base are tilted in opposite directions relative to the helix axis. As shown in the figure, the hydrocarbon is tilted such that the aliphatic end lies in the major groove toward the 5′ end of the adducted strand in the 10*S* adduct and toward the 3′ end of the adducted strand in the 10*R* adduct. In the 10*R* adduct duplex there is relatively little steric crowding between the hydrocarbon and the base pair to the 3′ side of the modified adenine, since this base pair is rotated (due to the right-hand helical twist) away from the aliphatic portion of the hydrocarbon.

In contrast, in the minor 10*S* adduct reported here, the right-handed helical twist causes the aliphatic end of the hydrocarbon to experience unfavorable steric interactions with the residue 5′ to the modified adenine. We speculate that this minor conformer of the duplex with a trans DE2-(10*S*) dA adduct in the normal, anti conformation opposite dG resembles an analogous, relatively unstable conformation (to date intractable to NMR structure determination) with dT in the complementary position. Rotation of the modified adenine (base paired with a dT) to the syn conformation to relieve steric crowding would also be relatively unfavorable, since it would not permit normal Watson−Crick base pairing. Thus, the 9-mer duplex with dT opposite a trans DE2(10*S*) dA adduct has a T_m of only 16 °C. Introduction of a dG mismatch opposite the modified dA* stabilizes the conformation in which the dA* has rotated to the syn conformation. Two base pair H-bonds are possible in the anti−syn dG-dA* mismatch pair, and the melting temperature (T_m = 28 °C) reflects this stabilization.

Speculations on the Relative Carcinogenicity of the Stereoisomers. The observation of multiple conformers for these DNA lesions may prove important, particularly if the minor conformers are those largely responsible for the adduct's carcinogenicity. The carcinogenicity of a given adduct may relate to mismatch incorporation, base deletion, or positive frame-shift mutation introduced into the DNA due to poor fidelity of the DNA polymerases in replicating past major or minor conformations (Christner et al., 1994; Moriya et al., 1996; Chary et al., 1997). Alternatively, carcinogenicity may relate to the inability of the DNA repair enzymes to recognize and repair lesions that can exist in various conformations (or a combination of poor polymerase fidelity/repair activity). Clearly, polymerization past the lesion block is competing with DNA lesion recognition and repair, and thus quite different relative degrees of polymerization fidelity could be expected for the major and minor conformers.

In both the major and minor adducts formed with the (+)-DE2 enantiomer, the mismatch dA_5*-dG_{14} base pair remains intact whereas in the adduct of the same base sequence with the less carcinogenic (−)-DE2, dA_5* and dG_{14} are no longer base paired and dG_{14} becomes extrahelical and "flipped out" (Schurter et al., 1995) (this is based upon the lack of any NOEs of the dG_{14} base to residues on either side, and thus no particular geometry can be inferred). In a number of recent crystal structures of various DNA repair enzyme−DNA duplex complexes, a base is found to "flip out" and insert into a cavity on the enzyme surface (Roberts, 1995). Thus in a pyrimidine photodimer DNA duplex bound to the DNA repair enzyme endo V (Vassylvey & Morikawa, 1995), the adenine ring opposite the photodimer lesion is flipped out into the enzyme. The enzyme thus recognizes the base opposite the lesion, not just the lesion itself. This may explain why the (+)-DE2 enantiomer (10*S* adduct) is more carcinogenic than the (−)-DE2 enantiomer as repair enzymes may be less apt to recognize a dA*-dG mismatch (resulting from misincorporation of dG by DNA polymerases) when the dG remains in the helix as opposed to a dA*-dG mismatch when the dG base is extrahelical. The result would be an increase in dA to dC transversions for DNA with the intercalated trans DE2(10*S*) dA adduct.

Conformational heterogeneity may also play a role in the relative carcinogenicity of the different stereoisomers. As indicated above, it appears to be generally true in the various dA lesion complexes that have been studied (Yeh et al., 1995; Schurter et al., 1995) that the most carcinogenic stereoisomers are those in which we observe the greatest conformational heterogeneity. Mutation of the DNA represents a balance between the fidelity of the polymerases in correctly recognizing the covalently modified base and the efficiency of the DNA repair enzymes to recognize the lesion, repair it, and allow polymerases to catalyze strand elongation through the lesion (or repaired lesion). A highly carcinogenic (and mutagenic) lesion must escape the repair enzymes and allow the polymerases to insert the incorrect base or create frame-shift mutations or deletions. Perhaps the heterogeneity and flexibility, as evidenced by the major and minor conformers of the (10*S*)-DE2 adduct, play a role in the relative ability of the various stereoisomeric adducts to cause cell transformation. While the polymerase may recognize the base lesion in one conformation, stalling long enough for DNA repair to occur at the site, it is conceivable that a lesion that is more flexible and that can take on alternate conformations will more readily permit the polymerase to insert the wrong base or cause a frame-shift or deletion mutation at the lesion site. However, until we have more definitive information on the structure of various polymerase and DNA repair enzyme complexes with DE-adducted DNA, it will not be possible to understand fully the basis of the relative carcinogenicity of these diol epoxides.

SUPPORTING INFORMATION AVAILABLE

Figures of the sequential connectivity diagrams (^{1}H base−H1′ region of 2D NOESY spectra) for both strands of the major and minor conformers, chemical shift assignments for both strands of the minor conformer, a structure determination statistics table, and an NOE table (15 pages). Ordering information is given on any current masthead page.

REFERENCES

Bax, A., & Davis, D. G. (1985) *J. Magn. Reson. 63*, 207−213.

Bothner-By, A., Stephens, R. L., & Lee, J. M. (1984) *J. Am. Chem. Soc. 106*, 811−813.

Chary, P., Harris, C. M., Harris, T. M., & Lloyd, R. S. (1997) *J. Biol. Chem. 272*, 5805−5813.

Christner, D. F., Lakshman, M. K., Sayer, J. M., Jerina, D. M., & Dipple, A. (1994) *Biochemistry 33*, 14297−14305.

Cosman, M., Fiala, R., Hingerty, B. E., Laryea, A., Lee, H. M., Harvey, R. G., Amin, S., Geacintov, N. E., Broyde, S., & Patel, D. (1993) *Biochemistry 32*, 12488−12497.

Cosman, M., Laryea, A., Fiala, R., Hingerty, B. E., Amin, S., Geacintov, N. E., Broyde, S., & Patel, D. J. (1995) *Biochemistry 34*, 1295−1307.

Fejzo, J., Westler, W. M., Macura, S., & Markley, J. L. (1991) *J. Magn. Reson. 92*, 20−29.

Ferrin, T. E., Huang, C. C., Jarvis, L. C., & Langridge, R. (1988) *J. Mol. Graphics 6*, 13−27.

Geacintov, N. E., Cosman, M., Hingerty, B. E., Amin, S., Broyde, S., & Patel, D. J. (1997) *Chem. Res. Toxicol. 10*, 111−146.

Jerina, D. M., Yagi, H., Thakker, D. R., Sayer, J. M., van Bladeren, P. J., Lehr, R. E., Whalen, D. L., Levin, W., Chang, R. L., Wood, A. W., & Conney, A. H. (1984) in *Foreign Compound Metabolism* (Caldwell, J., & Paulson, G. D., Eds.) pp 257−266, Taylor and Francis Ltd., London.

Jerina, D. M., Chadha, A., Cheh, A. M., Schurdak, M. E., Wood, A. W., & Sayer, J. M. (1991) *Biological Reactive Intermediates, IV. Molecular and Cellular Effects and their Impact on Human Health.*

Jerina, D. M., Sayer, J. M., Yeh, H. J. C., Liu, X., Yagi, H., Schurter, E., & Gorenstein, D. G. (1996) *Polycyclic Aromatic Compd. 10*, 145−152.

Macura, S., Westler, W. M., & Markley, J. L. (1994) in *Methods in Enzymology* (James, T. L., Ed.) Vol. 239, pp 106−144, Academic Press, New York.

Meadows, R., Post, C. B., Luxon, B. A., & Gorenstein, D. G. (1996) *MORASS.*

Moriya, M., Spiegel, S., Fernandes, A., Amin, S., Liu, T. M., Geacintov, N., & Grollman, A. P. (1996) *Biochemistry 35*, 16646−16651.

Pearlman, D. A., Case, D. A., Caldwell, J. C., Ross, W. L., Cheatham, T. E., Ferguson, D. M., Seibel, G. L., Singh, U. C., Weiner, P. K., & Kollman, P. A. (1995) *AMBER 4.1.*

Rance, M. (1987) *J. Magn. Reson. 74*, 557−564.

Roberts, R. J. (1995) *Cell 82*, 9−12.

Ross, W. S. (1994) *CARNAL.*

Schurter, E. J., Yeh, H. J. C., Sayer, J. M., Lakshman, M. K., Yagi, H., Jerina, D. M., & Gorenstein, D. G. (1995) *Biochemistry 34*, 1364−1375.

Vassylvey, D. G., & Morikawa, K. (1995) *Cell 83*, 773−782.

Wüthrich, K. (1986) *NMR of Proteins and Nucleic Acids*, John Wiley & Sons, New York.

Yeh, H. J. C., Sayer, J. M., Liu, X., Altieri, A. S., Byrd, R. A., Lashman, M. K., Yagi, H., Schurter, E. J., Gorenstein, D. G., & Jerina, D. M. (1995) *Biochemistry 34*, 13570−13581.

Zegar, I. S., Kim, S. J., Johansen, T. N., & Horton, P. J. (1996) *Biochemistry 35*, 6212−6224.

BI971306U